

# Retrievals of Aerosol Optical and Microphysical Properties from Imaging Polar Nephelometer Scattering Measurements

W. Reed Espinosa<sup>1,2</sup>, Lorraine A. Remer<sup>1,2</sup>, Oleg Dubovik<sup>3</sup>, Luke Ziemba<sup>4</sup>, Andreas Beyersdorf<sup>4,5</sup>, Daniel Orozco<sup>1,2</sup>, Gregory Schuster<sup>4</sup>, Tatyana Lapyonok<sup>3</sup>, David Fuertes<sup>6</sup>, and J. Vanderlei Martins<sup>1,2</sup>

<sup>1</sup>Department of Physics, University of Maryland Baltimore County, 1000 Hilltop Circle, Baltimore, MD 21250, USA

<sup>2</sup>Joint Center for Earth Systems Technology, University of Maryland Baltimore County, 5523 Research Park DR, Baltimore, MD 21228, USA

<sup>3</sup>Laboratoire d'Optique Atmosphérique, UMR8518, CNRS - Université de Lille 1, 59655, Villeneuve d'Ascq, France

<sup>4</sup>Langley Research Center Science Directorate, National Aeronautics and Space Administration, Hampton, Virginia, USA

<sup>5</sup>Department of Chemistry and Biochemistry, California State University San Bernardino, 5500 University Parkway, San Bernardino, CA 92407, USA

<sup>6</sup>GRASP-SAS, Bat-P5, Université de Lille 1, 59655, Villeneuve d'Ascq, France

*Correspondence to:* W. Reed Espinosa (reedespinosa@umbc.edu)

**Abstract.** A method for the retrieval of aerosol optical and microphysical properties from in situ light scattering measurements is presented and the results are compared with existing measurement techniques. The Generalized Retrieval of Aerosol and Surface Properties (GRASP) is applied to airborne and laboratory measurements made by a novel polar nephelometer. This instrument, the Polarized Imaging Nephelometer (PI-Neph), is capable of making high accuracy field measurements of phase function and degree of linear polarization, at three visible wavelengths, over a wide angular range of  $3^\circ$  to  $177^\circ$ . The resulting retrieval produces particle size distributions (PSDs) that agree, to within experimental error, with measurements made by commercial optical particle counters (OPCs). Additionally, the retrieved real part of the refractive index is generally found to be within the predicted error of 0.02 from the expected values for three species of humidified salt particles, whose refractive index is well established. The airborne measurements used in this work were made aboard the NASA DC-8 aircraft during the Studies of Emissions and Atmospheric Composition, Clouds and Climate Coupling by Regional Surveys (SEAC<sup>4</sup>RS) field campaign, and the inversion of this data represent the first aerosol retrievals of airborne polar nephelometer data. The results provide confidence in the real refractive index product, as well as in the retrieval's ability to accurately determine PSD, without assumptions about refractive index that are required by the majority of OPCs.

## 1 Introduction

Aerosols, and their interaction with clouds, play a key role in the climate of our planet. Additionally, measurements of aerosols are crucial to a wide range of direct applications, ranging from the monitoring of clean rooms to the impact of air quality on public health. Despite the importance of these particles, accurate in situ measurements of their optical and microphysical properties have remained a significant challenge.

Optical techniques of particle sizing typically capitalize on the approximately monotonic increase in the amount of light scattered by a single particle as a function particle size. These instruments are among the most widespread and precise available, but the vast majority of optical particle counter (OPC) designs require significant assumptions about the aerosol being sampled. These simplifications result from the limited information content present in typical OPC measurements, which frequently  
5 sample scattered light over a single angular range, often 4 to 22 degrees (Pinnick et al., 2000) or roughly 30 to 150 degrees (Cai et al., 2008) in so called wide angle OPCs. These assumptions, generally regarding real refractive index, absorption and particle morphology can lead to significant biases in the resulting particle size distributions (PSD) and generally constitute the bulk of the measurement error (Pinnick et al., 2000). Additionally, in situ measurements of many of these characteristics, like aerosol refractive index or particle sphericity for example, are still virtually nonexistent, especially at altitudes far from the  
10 surface.

A less common approach to characterizing particles is through polar nephelometer measurements of light scattering from an ensemble of particles over a large number of angular regions. This approach provides a large amount of information about the sample reducing the total number of assumptions required and the resulting biases in the retrieved products. Unfortunately, deploying field instruments with these capabilities can be quite challenging, and airborne measurements of common aerosols  
15 using this technique have previously been unavailable. Additionally, the inversion of multi-angular data, is significantly more complex than the inversion of light scattering intensity over a single angular range.

In spite of the complexities associated with multi-angle measurements and the corresponding inversions, there have been several successful attempts over the past four decades to retrieve particle properties from polar nephelometer data. The first published inversion of this kind was made by Eiden in 1966, who used multi-wavelength polarization data to retrieve the  
20 complex refractive index of an ambient aerosol, as well as match one of three predefined aerosol PSD models (Eiden, 1966). Jones et al. (1994) used intensity measurements to size monodisperse, polystyrene latex (PSL) spheres, as well as determine their complex index of refraction. Intensity and polarization measurements of ambient aerosols made by the Tohoku University single wavelength polar nephelometer in Sendai, Japan have been inverted to obtain complex refractive index and number concentrations in six log spaced size bins (Tanaka et al., 1983; Zhao, 1999). There have also been attempts to retrieve only the  
25 refractive index, while constraining the model's size distribution with a traditional particle sizer (Barkey et al., 2007, 2010). The converse approach was reported by Lienert et al. (2003), who took polarized measurements of sea spray and determined PSD by assuming a refractive index value expected for sodium chloride particles at the ambient relative humidity. Most recently, Sviridenkov et al. (2014) obtained both complex refractive index and PSD from three wavelength intensity measurements made with a commercially available polar nephelometer. All of these retrieval efforts have assumed spherical particles, and all  
30 measurements were made in the visible spectrum, except in the case of Jones et al. (1994) who used measurements made in the near-infrared. The only polar nephelometer retrievals to incorporate a non-spherical component in the scattering model were performed by Dubovik et al. (2006), who fit laboratory measurements of desert dust.

In this work we apply a complex inversion algorithm, specifically the Generalized Retrieval of Aerosol and Surface Properties (GRASP), to airborne and laboratory measurements made with the Polarized Imaging Nephelometer (PI-Neph), a multi-  
35 wavelength, multi-angle light scattering instrument. The GRASP retrieval makes no assumptions about the number of modes in

the size distribution or the complex refractive index, and it allows for both spherical and spheroidal scatterers. This represents a significant increase in complexity when compared to previous in situ scattering inversions. In addition to the generality of the retrieval, this work represents the first time that any aerosol retrieval algorithm has been applied to airborne polar nephelometer measurements. Furthermore, the ambient airborne measurements presented here were made in parallel to a large variety of independent instrumentation, allowing for very robust inter-comparisons of the retrieved products.

## 2 Inversion Methodology

Aerosol scattering matrix elements are measured in situ with a polar nephelometer and feed into a microphysical retrieval algorithm in order to obtain aerosol size distribution, complex refractive index ( $m$ ) and a percentage of spherical particles. These measurements include a combination of artificially suspended laboratory data as well as airborne data taken over the continental United States during the Studies of Emissions and Atmospheric Composition, Clouds and Climate Coupling by Regional Surveys (SEAC<sup>4</sup>RS) field experiment in 2013. GRASP, a versatile open source software package (<http://www.grasp-open.com>) capable of performing inversions on a wide variety of atmospheric optical measurements, was used to obtain the retrieved microphysical parameters. A detailed description of the GRASP retrieval algorithm and its capabilities can be found in Dubovik et al. (2011, 2014).

### 2.1 Polarized Imaging Nephelometer

In an effort to advance in situ characterization of atmospheric aerosols, the Laboratory for Aerosols, Clouds and Optics (LACO) at the University of Maryland, Baltimore County (UMBC) has developed a novel instrument concept called the Imaging Nephelometer (Dolgos and Martins, 2014). The imaging nephelometer design, first realized in the PI-Neph, uses a wide field of view charge coupled device (CCD) camera to image the light scattered by aerosols in the path of a high-powered continuous wave laser. This setup permits the construction of an instrument that is compact and stable enough to be flown on a variety of airborne platforms, while still allowing for measurements of scattering matrix elements over an angular resolution and range that is comparable to state of the art laboratory techniques (Muñoz et al., 2011).

A detailed schematic of the PI-Neph design is shown in Figure 1. The aerosol sample inside the PI-Neph is illuminated sequentially by a three wavelength laser system operating at 473nm, 532nm and 671nm. The three beams are aligned by a system of dichroics and mirrors before having their polarization state precisely oriented by a Glan-Taylor linear polarizer. A liquid crystal variable retarder (LCVR) and Fresnel Rhomb are then used to actively rotate the polarization state of laser light. After exiting the rhomb the beam is guided, by two mirrors, through a window into a 10 liter, sealed chamber containing the aerosol sample. The laser light traverses the length of the chamber before a corner cube retroreflector redirects the beam back into a beam trap adjacent to the entry window. The light scattered by the aerosol and surrounding gas is then imaged twice by the CCD camera, once for each of two roughly orthogonal linear polarization states of the laser.

If the scattering medium is assumed to be macroscopically isotropic and symmetric then the scattering matrix elements  $F_{13}$  and  $F_{14}$  do not contribute to the total scattered signal and the resulting pair of image intensities depend only on the first

two scattering matrix elements. The images can then be processed in a manner that allows for direct measurements of both the absolute phase function  $F_{11}(\theta)$  as well as  $F_{12}(\theta)$ , with  $\theta$  representing the zenith scattering angle (azimuthal symmetry is implied by the assumption of a macroscopically isotropic and symmetric medium). Measurements of molecular scatterers ( $CO_2$  and  $N_2$ ), whose absolute scattering matrix elements are well characterized (Anderson et al., 1996; Young, 1980), allow for the determination of unique calibration constants for each angle. This angular dependent absolute calibration allows for direct measurements of absolute phase function in known units ( $Mm^{-1}/sr$ ), free from any truncation error. The final products are then reported at standard temperature and pressure, with the Rayleigh scattering contribution from the surrounding gas subtracted. Additionally, normalized phases functions are represented by  $\tilde{F}_{11}$  in this paper and are scaled such that  $\tilde{F}_{11}(30^\circ) = 1$ .

The angular resolution of the measurement is limited by the spatial resolution of the CCD camera, the size of the camera's aperture and the width of the laser beam. The resulting raw resolution typically varies as a function of scattering angle ( $0.1^\circ < d\theta < 1^\circ$ ) but the final results are always binned to one degree. The angular range of the instrument is limited by stray light emanating from the entry and exit points of the laser beam. In the PI-Neph, an angular range of  $3^\circ$  to  $177^\circ$  in zenith scattering angle is frequently achieved.

PI-Neph measurements have been validated by a variety of methods since the instrument's completion in the summer of 2011. Measurements of monodisperse PSL spheres have yielded results that are in excellent agreement with Mie theory, while scattering coefficient measurements made in parallel with commercially available integrating nephelometers have agreed to within 5%. A detailed summary of PI-Neph design, calibration and validation can be found in Dolgos and Martins (2014).

## 2.2 Artificial Aerosol Generation

Ammonium sulfate ( $(NH_4)_2SO_4$ ), ammonium nitrate ( $NH_4NO_3$ ), and Sodium Chloride ( $NaCl$ ) were suspended and humidified in a laboratory setting. Figure 2 displays a schematic diagram of the particle generation and measurement setup. The salts were diluted with distilled water to a concentration of  $5g l^{-1}$  before being agitated with an ultrasonic vibrator and later suspended using a single jet atomizer (TSI, model 9302). The generated aerosol was diluted with filtered compressed air before being fed into a dryer and then a humidifier. In the first stage, generated particles are dried, without heating, to a relative humidity less than 30% using a Perma Pure Nafion dryer. The dry particles are later humidified to a  $RH > 80\%$  using two Perma Pure Nafion humidifiers (Nafion1 and Nafion2). The humidifier and dryer consist of a Nafion membrane tubing that transfers moisture to or from the surrounding medium. The drier uses compressed air while the air passing through Nafion 1 is humidified by flowing water and then used to humidify the sample passing through Nafion 2. The separation of liquid water from the Nafion tube in contact with the aerosol sample allows for subtler control of the final relative humidity (Orozco et al., 2016). Angular scattering measurements of the aerosol were then made by the PI-Neph before the sample was discharged from the system.

The humidification system was set to relative humidity values above the deliquescence points of each salt solution, typically to an RH just over 80%. The humidity was continuously monitored throughout the measurement using RH sensors located at the PI-Neph's inlet, measurement chamber, and outlet. The stability and reproducibility of the particle generation was

independently validated by the proper observation of deliquescence of different salts using an integrating nephelometer (model 3563, TSI Inc., St. Paul, MN, USA).

This setup was also used to suspend 903nm diameter monodisperse PSL spheres (Nanosphere 3900A, ThermoFisher Scientific, Fremont, CA, USA) and scattering measurements of these spheres were made by the PI-Neph at low relative humidities (RH < 20%). These measurements provide an opportunity to test the retrieval technique on an aerosol with a monodisperse size distribution and a refractive index that is very well characterized. The PSL generation and measurements also allowed for a small, sub-degree re-alignment of the PI-Neph scattering angle calibration in the case of the salt measurements. This correction was not applied to the data used in the PSL retrievals to avoid biasing the result.

### 2.3 Ambient Measurements

In addition to the laboratory measurements, inversions were performed on airborne data from the SEAC<sup>4</sup>RS experiment. SEAC<sup>4</sup>RS was a large field mission, that took place primarily over the continental United States, in August and September of 2013. Over the course of the experiment three aircraft flew 54 different instruments on a total of 57 flights in an effort to understand a broad range of atmospheric phenomenon. A detailed description of the scientific goals, aircraft and instrumentation, as well as the corresponding implementation can be found in Toon et al. (2016).

The PI-Neph made measurements aboard the NASA DC-8 aircraft during SEAC<sup>4</sup>RS. Ambient air was provided to the instrument through the NASA Langley Aerosol Research Group Experiment's (LARGE) shrouded diffuser inlet (McNaughton et al., 2007), which sampled isokinetically. A flow of 20 liters per minute was maintained through the PI-Neph's 10 liter sample chamber, leading to an aerosol exchange time on the order of 30 seconds. The raw sampling rate of the instrument was synchronized to match this interval, but the retrievals in this work are generally performed on time averages taken over a period of several minutes. The sample was conditioned with a temperature-controlled drier that heated the incoming ambient air to a temperature of 35°C and, in almost all cases, kept the relative humidity of the sample below 40%.

In addition to PI-Neph scattering measurements, the LARGE group made comprehensive in situ measurements of aerosol properties in parallel to the PI-Neph. These measurements, containing data on particle number density, size distribution and optical properties, are a valuable resource for the inter-comparison of PI-Neph measurements and the corresponding retrieved microphysical properties. In this work PI-Neph retrieved size distributions will be compared extensively to measurements made by two dedicated optical particle size spectrometers (LAS model 3340, TSI Inc., St. Paul, MN, USA and model UHSAS, Droplet Measurement Technologies, Boulder, CO, USA) as well as an aerodynamic particle sizer (APS model 3321, TSI Inc., St. Paul, MN, USA). The two optical particle spectrometers also measured at low relative humidities during SEAC<sup>4</sup>RS, but their sample was conditioned through a drier. This approach minimizes the evaporation of volatile compounds but can also lead to size dependent losses in the aerosol when the instrument requires relatively large flow rates, as is the case for the PI-Neph. The aerodynamic particle sizer measurements were made at ambient humidities, but the ambient RH was determined to be less than 40% in all cases shown here so differences in PSD resulting from hygroscopic growth are not expected.

Fifty separate sampling periods, occurring over the course of ten different flights, are highlighted in this work. The flights selected represent the ten days with the highest quality PI-Neph data, for which data is available for at least one of LARGE's

dedicated particle sizers. The intervals containing the highest aerosol scattering levels during these flights were identified and a robust averaging procedure (Beaton and Tukey, 1974) was applied to periods for which no detectable changes in the normalized angular scattering data was observed. The total scattering for these averages ranged from  $30\text{Mm}^{-1}$  to just over  $500\text{Mm}^{-1}$ , with a median value of  $90\text{Mm}^{-1}$ . The resulting dataset represents a wide range of aerosols, including urban pollution, organics, Saharan dust and over a dozen cases dominated by biomass burning (BB) emissions with transport ages ranging from hours to several days.

Additionally, three individual case studies were selected to provide detailed examples of PI-Neph measurements, the corresponding GRASP fit and the resulting retrieved size distributions. Two of these cases come from periods where the scattering signal was dominated by forest fire emissions, and were chosen to emphasize the subtle distinctions in angular scattering patterns that can occur, even between two aerosols of similar type. The third case consists of boundary layer (BL) measurements made over a heavily forested region of south east Missouri. This case represents one of only a couple of periods in which a significant coarse mode was observed. The sampling locations of these three cases, as well as the flight paths for the ten selected flights, are shown in Figure 3.

## 2.4 Implementation of GRASP Retrieval

GRASP is a versatile software package capable of retrieving a wide range of atmospheric and surface properties from a variety of datasets. The GRASP algorithm and corresponding software builds on the successful heritage of the PARASOL (Dubovik et al., 2011), AERONET (Dubovik and King, 2000) and laboratory (Dubovik et al., 2006) retrievals.

GRASP's base aerosol model contains very few assumptions in comparison with traditional in situ or remote sensing retrieval algorithms. It includes all necessary components required to simulate a diverse range of atmospheric observations, including remote sensing (both suborbital and space-based), optical in situ and laboratory measurements. The settings of the retrieved characteristics can be flexibly adjusted to match the particular application. For example, aerosol size distribution can be represented as a superposition of several log-normal functions or as a binned continuous function with different size resolutions (it is defined in nodal points).

As an inversion concept GRASP implements Multi-Term Least Square fitting (Dubovik, 2004). This approach allows for convenient combining of different types of observations and multiple a priori constraints in a single inversion. For example, following this concept the AERONET retrieval (Dubovik and King, 2000) retrieves many parameters simultaneously: aerosol size distribution, spectral complex refractive index and fraction of spherical particles. A priori constraints on all functions (size distribution and all spectral dependencies) are assumed smooth, while a priori estimates of values are also used for some parameters. Moreover, using the same strategy a statistically optimized multi-pixel retrieval concept was realized as an option in GRASP (Dubovik et al., 2011). This concept uses additional a priori knowledge about time and space variability of the retrieved parameters in the inversion of coordinated observations (i.e. satellite observations in different pixels).

The flexibility built into the design of GRASP allows the user to select the assumptions that best match the information content of a particular dataset. Moreover, while all of the above features have never been used in one single application, they often provide important potential for evolution of each application, for example via implementing synergy retrievals using a

combination of different observations. The GRASP algorithm has previously been successfully applied to both satellite and ground-based upward-looking sky radiance measurements (Dubovik et al., 2011, 2014; Xu et al., 2016), while this paper represents the first application of GRASP to polar nephelometer data.

In this work GRASP size distributions were modeled with 16 logarithmically spaced size bins, generally ranging from 50nm to 2.94 $\mu$ m in radius. The lower end of this range corresponds to the sensitivity limit of ensemble type, light scattering measurements, given realistic particle size distributions. The upper bound was chosen to include the vast majority of coarse mode particles capable of passing through the LARGE inlet, which has a 50% passing efficiency at an aerodynamic radius of 1.8 $\mu$ m (McNaughton et al., 2007). This size range was reduced to radii between 425nm and 476nm in the case of the PSL spheres, in order to better capture the fine structure of their very narrow size distribution. In all retrievals the shape of the size distribution is only constrained by a smoothness parameter and no assumptions about the number of modes are made.

The search space for the real part of the refractive index ( $n$ ) is semi-continuous between 1.33 and 1.68, while the imaginary part ( $k$ ) can range from 0 to  $10^{-1}$ . The refractive index is held constant with respect to size but is allowed to vary as a function of wavelength. GRASP's aerosol model assumes a mixture of spheres and spheroids, whose axis ratio distribution is fixed and derived from feldspar measurements made by Volten et al. (2001). It can be shown that small deviations in the spheroid component's axis ratio distribution produces negligible changes in the angular dependence of the scattered light (Dubovik et al., 2006). It is therefore believed that this fixed shape distribution is capable of accurately modeling a wide range of non-spherical aerosols. The spheroid component was omitted from the PSL retrievals due the computational demands associated with generating the required precomputed kernels for the finer size parameter grid spacing.

### 3 Retrieval Results and Discussion

#### 3.1 Measured Data and Retrieval Fit

In both the 50 selected SEAC<sup>4</sup>RS cases and in the laboratory measurements, the residuals between the GRASP fits and the PI-Neph measured values are generally within the PI-Neph instrumental error. Figure 4 shows the measured and fit  $F_{11}$  and  $-F_{12}/F_{11}$  for the ammonium sulfate case, and is typical of the bulk of the retrievals performed in this work. The residuals are also plotted to clearly emphasize the differences between the measurement and fit relative to the instrument's  $2\sigma$  error. In the case of the  $F_{11}$  data the distances between the fit and measured values are reported as:

$$RES_{F_{11}} = \text{Log}_{10}(F_{11}^{MEAS}) - \text{Log}_{10}(F_{11}^{FIT}) \quad (1)$$

with the PI-Neph error transformed accordingly. This transformation provides a measure of relative (as opposed to absolute) error, and provides a consistently sized metric across the two orders of magnitude covered by  $F_{11}$ . The separation in  $-F_{12}/F_{11}$  data is represented simply as the difference between the measured and fit values.

$$RES_{F_{12}/F_{11}} = \left(\frac{F_{12}}{F_{11}}\right)^{FIT} - \left(\frac{F_{12}}{F_{11}}\right)^{MEAS} \quad (2)$$

Figure 5 shows the normalized scattering matrix elements at 532nm for the three selected SEAC<sup>4</sup>RS case studies. A strong forward peak can be seen in the forest boundary layer measurements, which is in accordance with the significant coarse mode observed by the aerodynamic and optical particle sizers. The two biomass burning cases display very similar  $F_{11}$  values, with the only significant difference being slightly enhanced forward and backward scattering in BB Plume #2. These subtle differences are likely driven by the slightly larger fraction of coarse mode particles present in the latter case. In contrast to  $F_{11}$ ,  $-F_{12}/F_{11}$  shows significant differences between the two biomass burning cases. The reduced magnitude of  $-F_{12}/F_{11}$  in BB Plume #1 is likely driven primarily by differences in real refractive index between the two samples. This hypothesis is supported by simulations with a Mie code (Mishchenko et al., 2002) which demonstrated that, in the relevant size regime, changes in refractive index on the order of 0.03 had little effect on  $F_{11}$  but could easily change the ratio of  $F_{12}$  to  $F_{11}$  by 20% or more. It is this effect, in combination with the small median size of the fine mode, that produces the highest degree of linear polarization of the three samples in the forested boundary layer case.

The spectral dependence of  $F_{11}$  and  $-F_{12}/F_{11}$  for the biomass burning case study sampled on August 19<sup>th</sup> is shown in Figure 6. The absolute phase function values are shown here to emphasize the additional information present in the spectral dependence of the scattering intensities. It should be noted that there is also significant spectral dependence in the shape of the scattering matrix elements, particularly in  $-F_{12}/F_{11}$ . These difference are driven primarily by changes in size parameter, but also result in some part from a non-zero spectral dependence of the complex refractive index. The same variables are plotted for the the forested boundary layer case in Figure 7 to show the spectral dependence of the measured scattering matrix elements and the corresponding fits when a significant coarse mode is present. In this last case, low aerosol concentrations and greater than average straylight levels inside the instrument resulted in a gap in the 473nm  $F_{12}$  measurements between 80° and 142° in scattering angle.

In the case of the polydisperse samples, the oscillations occasionally present in the data over angular scales of roughly ten degrees are likely non-physical, and artifacts of insufficient sampling statistics in the coarse mode. The extended length of the imaging nephelometer sample volume makes it especially susceptible to sampling statistic artifacts that are produced by the largest particles. These particles make up a very small fraction of the total number concentration, while simultaneously accounting for a disproportionately large portion of the total scattered light. This is especially apparent in the measurements of  $-F_{12}/F_{11}$  as these values are closely related to the differences between sequential measurements at different polarizations. A large particle that is present at a given location in one image, but not present in the corresponding adjacent image will produce a significant artifact. The effect is also evident at low scattering angles, where larger particles tend to represent a larger portion of total scattering.

The monodisperse PSL measurements and corresponding GRASP fits (shown in Figure 8) agree well in the case of  $F_{11}$ . Overall there is also good agreement in the  $-F_{12}/F_{11}$  data, but some significant deviations do occur. The GRASP size distribution retrieval for this case had a full width, 67 percentile (FW67) of 17nm, which is more than twice the width specified by the manufacturer (FW67=8.2nm). However, a narrower size distribution corresponding to the manufacturer's specification was found to reproduce some features of the measurement significantly better than GRASP's original retrieval. This improvement was most apparent in the 473nm and 532nm  $-F_{12}/F_{11}$  data, particularly at scattering angles between 20° and 60° where Mie

theory predicts  $-F_{12}/F_{11}$  to have high sensitivity to the distribution's width. Further studies indicated that GRASP was able to reproduce  $-F_{12}/F_{11}$  corresponding to this narrower PSD with high accuracy when noise free synthetic data was used as input. Additionally, running retrievals on the measured data using increasingly finer size resolution kernels did not improve the retrieval's ability to fit these features. The deviations in the fit were thus determined to be the result of GRASP's sensitivity to certain characteristics of the noise in the measured data, not insufficient size resolution in the fine resolution kernels used in the PSL case.

### 3.2 Refractive Index Retrievals

Crystalline particles do not take on water until reaching relative humidities above their deliquescence point, generally around 80% in the case of salts. A range of methods are available for calculating the size of a given salt droplet, after the transformation to an aqueous state has been made. In this work we choose the parameterization proposed by Petters and Kreidenweis (2007) for its simplicity and because the required  $\kappa$  parameters are well known for the salts in question. This method states that  $gf_{vol}$ , the volume growth factor of a particle, can be estimated as:

$$gf_{vol}(RH) = 1 + \kappa \frac{RH}{1 - RH} \quad (3)$$

where RH is the relative humidity of the air surrounding the droplet and  $\kappa$  is a constant that is determined by the composition of the particle in question.

The dry (crystalline) refractive indices of all three salts studied in this work are well known (Tang, 1996) and the resulting wet refractive index can be calculated from the volume mixing rule:

$$n_{wet}(RH) = \frac{(gf_{vol} - 1)n_{H_2O} + n_{dry}}{gf_{vol}} \quad (4)$$

where  $n_{H_2O}$  is the refractive index of water,  $n_{dry}$  is the refractive index of the dry salt and  $n_{wet}$  is the refractive index of the solution (Nessler et al., 2005). Alternative methods for estimating the refractive index of hygroscopic particles exist, but their deviation from the volume mixing rule is less than 1% for solutions that are made up of more than 50% water (Erlick et al., 2011; Schuster et al., 2009).

The refractive indices predicted from equations 3 and 4 are compared with the corresponding GRASP retrievals in Table 1. The ranges of  $\kappa$  values given for sodium chloride and ammonium sulfate are taken from Table 3 of Koehler et al. (2006) and were derived from hygroscopic growth factors in the sub-saturated domain. The  $\kappa$  range used for ammonium nitrate are derived from measurements of cloud condensation nuclei (CCN), at super-saturations less than 1%, and originate from Svenningsson et al. (2006), with the spread representing an uncertainty of one standard deviation. Growth factor derived  $\kappa$  values were not available for ammonium nitrate but the difference between growth factor and CCN derived  $\kappa$  values is generally small compared to the uncertainty in  $\kappa$  resulting from measurement errors (Petters and Kreidenweis, 2007). The range in the final predicted wet refractive indices results from the bounds on the  $\kappa$  values, as well as a 2% uncertainty in the RH measurement made inside the PI-Neph.

The retrieved refractive index values are in good agreement with the range predicted by  $\kappa$ -Köhler theory and the existing literature. Sensitivity studies, performed on ensembles of synthetic data perturbed with modeled PI-Neph noise, suggest one standard deviation uncertainties in retrieved real refractive indices of around 0.02 for non-absorbing particles in the size range of these humidified salts. These studies also showed a general trend of increasing accuracy in the retrieved real part of the refractive index as the median radius of the particles increased. The converse was true for absorption, where more absorbing particles tended to produce more error in the real refractive index inversion. The agreement between the retrieved and predicted refractive index values is consistent with this error analysis.

The retrieved imaginary parts of the refractive index (not shown) of the ammonium nitrate and ammonium sulfate solutions were both found to be on the order of  $10^{-3}$ . These values are indicative of moderate absorption but are larger than more established values found in the existing literature, which suggests very little absorption ( $k < 10^{-7}$ ) for all three of the solutions measured (Fenn et al., 1985; Toon and Pollack, 1976; Hale and Querry, 1973). An even higher imaginary part of the refractive index ( $k = 0.026$ ) was retrieved in the case of the sodium chloride sample. The magnitude of this value may be, at least in part, related to an unrealistically high retrieved real refractive index. This hypothesis is supported by the fact that constraining the retrieved real refractive index to the range predicted by the sample RH and  $\kappa$ -Köhler theory resulted in significantly lower retrieved values of sodium chloride absorption. A comparison was also made between the retrieved single scattering albedo (SSA) and the SSA derived from Particle Soot/Absorption Photometer (PSAP, Radiance Research, Seattle, WA, USA) and integrated scattering measurements (Integrating Nephelometer 3563, TSI Inc., St. Paul, MN, USA) in SEAC<sup>4</sup>RS. A statistically significant correlation between the two data sets was determined to exist, but the retrieved SSA was also found to systematically overestimate the measured absorption. Notice that the retrieval was based only on scattering measurements (no absorption or extinction data was included) and therefore is expected to show limited sensitivity to these variables. A detailed analysis of the sensitivity of the GRASP/PI-Neph retrieval to absorption is beyond the scope of this work.

After passing their deliquescence point, crystalline salt particles should transform into saline droplets and become spherical in shape. The GRASP/PI-Neph inversion was able to accurately reproduce this spherical morphology in the sodium chloride and ammonium sulfate case, but a spherical fraction of only 54% was retrieved for the ammonium nitrate sample. This deviation from expectation is likely driven by a combination of random error in the PI-Neph measurement and the fact that the scattering of non-spherical particles tends to deviate less from that of spherical particles as particle size decreases. This notion is confirmed in the sensitivity studies previously described, where it was found that there was very little sensitivity to sphericity in the case of small particles ( $r < 200\text{nm}$ ).

Retrievals of the monodisperse PSL spheres produced real refractive index values that were within the range of existing measurements available in the literature at all three wavelengths (Bateman et al., 1959; Ma et al., 2003; Sultanova et al., 2003; Jones et al., 2013). The spectral dependence of the retrieved values, as well as the three most recently reported Cauchy Equation parameterizations of PSL refractive index can be found in Figure 9. The retrieved imaginary part of the refractive index for these spheres was on the order of  $10^{-3}$  for all three wavelengths, slightly higher than the values of around  $4 \times 10^{-4}$  that have been reported by more sensitive techniques (Bateman et al., 1959; Ma et al., 2003).

Figure 10 shows the spectrally dependent distribution of the retrieved dry refractive indices for the 50 chosen SEAC<sup>4</sup>RS cases. The mean retrieved real part of the refractive index at 532nm for the 50 cases, composed primarily of biomass burning and urban-biogenic mixtures, was found to be 1.53. This figure is in line with the existing measurements made under similar conditions (Shingler et al., 2016), but unfortunately very few airborne, in situ measurements of refractive index are available.

5 Remote sensing retrievals of biomass burning aerosol generally range from 1.47 to 1.55 (Dubovik et al., 2002; Li and Mao, 1990; Westphal and Toon, 1991; Yamasoe et al., 1998), while remote retrievals of urban pollution have generally yielded somewhat lower values, ranging from 1.39 to 1.46 (Dubovik et al., 2002; Redemann et al., 2000). These lower values observed in the urban pollution remote sensing retrievals are likely driven in large part by particle hygroscopicity. The PI-Neph/GRASP retrievals of real refractive index are expected to be significantly higher in analogous cases as the PI-Neph measurements

10 were made at very low relative humidities, where hygroscopic growth is virtually non-existent. In spite of these differences in measurement conditions, as well as in the sample regions in question, the values are remarkably similar, especially in the case of biomass burning emissions, where hygroscopic influences are expected to be much more limited. Additionally, the spectral dependence is in line with expectation, and closely matches measurements of common natural aerosol constituents made by Hale and Querry (1973).

15 Table 2 shows details of the retrievals performed on the three cases studies. The retrieved real refractive index of the August 19<sup>th</sup> biomass burning plume is slightly higher than the values reported in the literature, and represents the upper end of the values retrieved in the 50 selected samples. The other two cases also returned higher than average values, although they were more in line with the other samples and typical values reported in the existing literature. The biomass burning particles were also found to be less absorbing than that of typical smoke, but the values produced by GRASP are in good agreement with direct

20 SSA measurements aboard the DC-8 derived from PSAP and integrating nephelometer measurements (SEAC<sup>4</sup>RS, 2015). A significant percentage of particles were determined to be non-spherical in these cases, especially the August 19<sup>th</sup> biomass burning plume and August 30<sup>th</sup> forested boundary layer aerosols. The cases on August 19<sup>th</sup> and August 27<sup>th</sup> are dominated by small particles, and in turn there are large uncertainties in the sphericity product. The low spherical percentage retrieved for the August 30<sup>th</sup> case is potentially realistic given the significance of the coarse mode, but additional independent measurements of

25 sphericity are limited.

### 3.3 Size Distribution Retrievals

The size distribution retrieved for the PSL spheres is shown in the sub-panel of Figure 9 and agrees well with the manufacturer's specifications. The median diameter of the retrieved distribution was found to be 902.7nm which shows excellent agreement with the manufacturer's NIST traceable specification of 903nm±12. It is the authors' experience, based on PI-Neph

30 measurement inversions on a range of PSL products from the same manufacturer, that the uncertainty listed often significantly overestimates the true uncertainty in the central diameter of the size distribution. As discussed in Section 3.1, the retrieval returned a distribution width that was approximately twice the value specified by the manufacturer but features in the  $-F_{12}/F_{11}$  measurement indicate that the true width is more likely inline with the manufacturer's specification FW67 of 8.2nm. Similarly

accurate results sizing PSL spheres with PI-Neph data are demonstrated in Dolgos and Martins (2014) through the use of a Mie theory lookup table.

The retrieved size distributions for all three SEAC<sup>4</sup>RS case studies are plotted alongside measurements made by dedicated particle sizers in Figure 11. The APS data was converted from aerodynamic to geometric size using an assumed density of 1.3gcm<sup>-3</sup> and a shape factor of unity. Uncertainties in these assumption can generate significant changes in the resulting geometric PSD, but the presence of APS data can still be used as an optically independent, qualitative confirmation regarding the presence of significant coarse mode. The UHSAS data is shown for two different calibration aerosols, PSL spheres and ammonium sulfate, which have real refractive indices of 1.61 (Jones et al., 2013) and 1.53 (Tang, 1996) respectively. The LAS data shown corresponds to calibration with PSL spheres.

In all three of these cases the peak of the fine mode generally occurs around a radius of 150nm. These values are typical of the majority of the 50 selected periods, all of which have fine mode median radii (in volume) between 100nm and 200nm. The PI-Neph/GRASP PSD retrievals fall between the two different UHSAS calibrations in each of the three cases, which again is typical of almost all 50 samples.

Among the 50 selected periods for which size distribution comparisons were made, only two cases had coarse modes with volume concentrations that made up a significant portion of the total particle volume. The first of these cases, a sample dominated by transported Saharan dust, had very low aerosol loading and the bulk of the scattering matrix data at scattering angles above 40° was below the PI-Neph's limit of detection. The second of these cases, the forested boundary layer measurements taken on August 30<sup>th</sup>, was therefore chosen as one of the three highlighted case studies. In both cases the size distributions agree remarkably well in the coarse mode, suggesting significant sensitivity to larger particles in the retrieved product. This sensitivity likely resulted primarily from the PI-Neph's ability to measure down to scattering angles as low as 3° during SEAC<sup>4</sup>RS. Lienert et al. (2003) was also able to show sensitivity to super-micron particles given a minimum scattering angle of around 2°. On the other hand, Sviridenkov et al. (2014) determined that single scattering measurements over a scattering angle range of 10° to 90°, were insufficient to provide significant information about the coarse mode. All of these conclusions are in agreement with theoretical sensitivity studies indicating that measurements at very low scattering angles are required if the coarse mode is to be accurately recovered (Dubovik et al., 2000).

In order to simplify the comparison of the retrieved size distributions with those measured by the dedicated aerosol spectrometers, the fine mode of each PSD was parameterized according to three metrics: total volume concentration, median radius and the span of the distribution. When determining these metrics the values of the volume distributions corresponding to radii less than 50nm were first removed, as this lower bound corresponds to the bottom of the PI-Neph/GRASP retrieval range. The upper end of the remaining size distribution was then further truncated to include only fine mode particles. The division between the fine and coarse modes was defined as the minimum value of the LAS volume distribution, closest to r=300nm. A visual inspection of all cases confirmed that this metric was sufficient to reasonably isolate the fine mode when two modes were present. The volume concentration, median ( $r_{50}$ ) and span ( $(r_{90} - r_{10})/r_{50}$ ) were then calculated using these final truncated volume distributions. Linear interpolation was used when the 10<sup>th</sup>, 50<sup>th</sup> or 90<sup>th</sup> percentile values, as well as the bounds of the

truncated distributions, fell between the midpoints of two size bins. Scatter plots showing the results of these parameterizations for the three OPC measurements vs the corresponding PI-Neph retrieval are shown in Figure 12.

The PI-Neph retrieved volume concentrations and median radii generally fall somewhere between the two different UHSAS calibrations, with the best agreement generally tending towards the ammonium sulfate calibration. This is consistent with the  
5 average retrieved refractive index for the 50 cases ( $n=1.53$ ) which is in very close agreement to the dry refractive index of ammonium sulfate found in the literature. The LAS consistently measured smaller and fewer particles than all the other sizing techniques, but still showed significant correlation with the PI-Neph/GRASP retrievals. There was weaker agreement regarding the width of the distribution among the four techniques. The retrieved spans generally best matched the corresponding PSL calibrated UHSAS values, but the values covered a larger range of spans than the values measured by the OPCs. The PI-Neph  
10 retrieved spans fell between 0.55 and 1.03 in 95% of the cases. In contrast, the LAS showed the least variability in span, with 95% of the values falling between 0.65 and 0.85. The differences in span between PI-Neph retrievals and the OPCs was likely driven in large part by their different sampling techniques (ensemble vs single particle measurements).

The large differences between UHSAS measurements under different calibrations, with disparate refractive indices, demonstrates the significance of the refractive index assumptions required. The results of this work, as well as others (Shingler et al.,  
15 2016), suggest that the real refractive indices of natural aerosol can frequently reach values as low as 1.48 at 532nm. This is substantially lower than the refractive index of ammonium sulfate ( $n = 1.53$ ), which has the lowest value of the aerosols that are commonly used to calibrate optical particle sizers, and further emphasizes the significance of the basis resulting from uncertainty in refractive indices.

In order to further assess the retrieval variability, resulting from changes in refractive index and sphericity, the 50 SEAC<sup>4</sup>RS  
20 cases were inverted a second time with assumptions corresponding to PSL spheres. In this analysis the complex refractive index was forced match measurements of PSL and non-spherical particles were excluded from GRASP's aerosol model. This configuration produced significantly better agreement with the PSL calibrated UHSAS measurements in volume concentration, median radius and span, when compared to the unconstrained retrievals. This result further demonstrates that differences in fundamental assumptions about the optical and morphological properties of the particles are driving a significant portion of the  
25 differences between the retrieved and measured values.

#### 4 Conclusions

This work represents the first time that aerosol optical and microphysical properties were retrieved from airborne, polar nephelometer data. Additionally, the PI-Neph/GRASP inversion makes fewer assumptions regarding the shape of the recovered size distribution and particle sphericity than previous in situ light scattering retrievals. The resulting products are in good agreement  
30 with expectations, and compare well with existing measurement techniques. Furthermore, the GRASP fit to PI-Neph data is consistent with the PI-Neph's level of error, indicating that the assumptions made in the retrieval are sufficient to faithfully reproduce the light scattering of realistic, ambient aerosols.

The real refractive index of humidified salts retrieved with this method agree well with the predictions made by  $\kappa$ -Köhler theory and existing dry measurements. The PI-Neph retrieval of PSL refractive index agrees with other contemporary techniques to within the deviation present in those reported values. Furthermore, inversions of airborne SEAC<sup>4</sup>RS data produced refractive indices that were in good agreement with the existing literature.

5 There is significant spread in the aerosol size distribution measurements made by the OPCs, but the corresponding PI-Neph/GRASP retrievals generally fall within the range of the existing measurements. A major part of the differences in the measured size distributions stem from the need to assume a refractive index during the calibration process. The PI-Neph/GRASP retrieval has sufficient sensitivity to constrain the refractive index with enough accuracy to potentially reduce these biases. The fact that the PSD retrievals fell between the two UHSAS calibrations, in a manner consistent with the retrieved refractive index,  
10 supports this conclusion.

The PI-Neph inversions have also shown moderate sensitivity to absorption but a detailed assessment of the accuracy of this retrieved parameter is beyond the scope of this paper and will have to remain the subject of future study. Additionally, promising results were obtained regarding the retrieval of sphericity in the case of the humidified salts as well as in sensitivity studies, but as a result of the limited morphological information available in the SEAC<sup>4</sup>RS dataset, a robust evaluation of this  
15 product is limited at this time.

## 5 Code availability

The GRASP software package is open-source and available for download by request at <http://www.grasp-open.com>.

## 6 Data availability

All relevant measurements made during the SEAC<sup>4</sup>RS experiment are available through the SEAC<sup>4</sup>RS data archive at <http://www-air.larc.nasa.gov/missions/seac4rs/> (SEAC4RS, 2015). Requests for additional data can be made to the corresponding author at [reedespinosa@umbc.edu](mailto:reedespinosa@umbc.edu).  
20

*Acknowledgements.* We acknowledge funding support from the NASA Earth Science Enterprise for the SEAC<sup>4</sup>RS campaign under Grant NNX12AC37G, and under the Atmospheric Composition Campaign Data Analysis and Modeling Program (ACCDAM) grant NNX14AP73G, both managed by Dr. Hal Maring. The authors would also like to thank the members of the LARGE group, particularly Bruce Anderson,  
25 Edward Winstead and Lee Thornhill for their support incorporating the PI-Neph into the LARGE instrument package. We are also grateful for the scientific and technical support of the LACO team at UMBC, especially Dominik Cieslak and Frank Harris. Additionally, we would like to thank the entire SEAC<sup>4</sup>RS science team for providing supporting data and relevant discussion.

## References

- Anderson, T. L., Covert, D. S., Marshall, S. F., Laucks, M. L., Charlson, R. J., Waggoner, A. P., Ogren, J. A., Caldow, R., Holm, R. L., Quant, F. R., Sem, G. J., Wiedensohler, A., Ahlquist, N. A., and Bates, T. S.: Performance Characteristics of a High-Sensitivity, Three-Wavelength Total Scattering/Backscatter Nephelometer, *Journal of Atmospheric and Oceanic Technology*, 13, 967–986, 1996.
- 5 Barkey, B., Paulson, S. E., and Chung, A.: Genetic Algorithm Inversion of Dual Polarization Polar Nephelometer Data to Determine Aerosol Refractive Index, *Aerosol Science and Technology*, 41, 751–760, doi:10.1080/02786820701432640, 2007.
- Barkey, B., Kim, H., and Paulson, S. E.: Genetic Algorithm Retrieval of Real Refractive Index from Aerosol Distributions that are not Lognormal, *Aerosol Science and Technology*, 44, 1089–1095, doi:10.1080/02786826.2010.512025, 2010.
- Bateman, J., Weneck, E., and Eshler, D.: Determination of particle size and concentration from spectrophotometric transmission, *Journal of*  
10 *Colloid Science*, 14, 308–329, doi:10.1016/0095-8522(59)90055-8, 1959.
- Beaton, A. E. and Tukey, J. W.: The Fitting of Power Series, Meaning Polynomials, Illustrated on Band-Spectroscopic Data, *Technometrics*, 16, 147–185, doi:10.2307/1267936, 1974.
- Cai, Y., Montague, D. C., Mooiweer-Bryan, W., and Deshler, T.: Performance characteristics of the ultra high sensitivity aerosol spectrometer for particles between 55 and 800 nm: Laboratory and field studies, *Journal of Aerosol Science*, 39, 759–769,  
15 doi:10.1016/j.jaerosci.2008.04.007, 2008.
- Dolgos, G. and Martins, J. V.: Polarized Imaging Nephelometer for in situ airborne measurements of aerosol light scattering, *Optics Express*, 22, 21 972–21 990, doi:10.1364/OE.22.021972, 2014.
- Dubovik, O.: Optimization of Numerical Inversion in Photopolarimetric Remote Sensing, *Photopolarimetry in Remote Sensing*, pp. 65–106, doi:10.1007/1-4020-2368-5\_3, 2004.
- 20 Dubovik, O. and King, M.: A flexible inversion algorithm for retrieval of aerosol optical properties from Sun and sky radiance measurements, *Journal of Geophysical Research*, 105, 20,673–20,696, 2000.
- Dubovik, O., Smirnov, a., Holben, B. N., King, M. D., Kaufman, Y. J., Eck, T. F., and Slutsker, I.: Accuracy assessments of aerosol optical properties retrieved from Aerosol Robotic Network (AERONET) Sun and sky radiance measurements, *Journal of Geophysical Research: Atmospheres*, 105, 9791–9806, doi:10.1029/2000JD900040, 2000.
- 25 Dubovik, O., Holben, B., Eck, T., Smirnov, A., Kaufman, Y., and King, M.: Variability of absorption and optical properties of key aerosol types observed in worldwide locations, *Journal of the Atmospheric Sciences*, 59, 590–608, 2002.
- Dubovik, O., Sinyuk, A., Lapyonok, T., Holben, B. N., Mishchenko, M., Yang, P., Eck, T. F., Volten, H., Muñoz, O., Veihelmann, B., van der Zande, W. J., Leon, J.-F., Sorokin, M., and Slutsker, I.: Application of spheroid models to account for aerosol particle nonsphericity in remote sensing of desert dust, *Journal of Geophysical Research*, 111, D11 208, doi:10.1029/2005JD006619, 2006.
- 30 Dubovik, O., Herman, M., Holdak, a., Lapyonok, T., Tanré, D., Deuzé, J. L., Ducos, F., Sinyuk, a., and Lopatin, a.: Statistically optimized inversion algorithm for enhanced retrieval of aerosol properties from spectral multi-angle polarimetric satellite observations, *Atmospheric Measurement Techniques*, 4, 975–1018, doi:10.5194/amt-4-975-2011, 2011.
- Dubovik, O., Lapyonok, T., Litvinov, P., Herman, M., Fuertes, D., Ducos, F., Torres, B., Derimian, Y., Huang, X., Lopatin, A., Chaikovskiy, A., Aspetsberger, M., and Federspiel, C.: GRASP: a versatile algorithm for characterizing the atmosphere, *SPIE Newsroom*, pp. 2–5,  
35 doi:10.1117/2.1201408.005558, 2014.
- Eiden, R.: The elliptical polarization of light scattered by a volume of atmospheric air., *Applied optics*, 5, 569–75, 1966.

- Erlick, C., Abbatt, J. P. D., and Rudich, Y.: How Different Calculations of the Refractive Index Affect Estimates of the Radiative Forcing Efficiency of Ammonium Sulfate Aerosols, *Journal of the Atmospheric Sciences*, 68, 1845–1852, doi:10.1175/2011JAS3721.1, 2011.
- Fenn, R. W., Clough, S. a., Gallery, W. O., Good, R. E., Kneizys, F. X., Mill, J., Rothman, L., Shettle, E., and Volz, F.: Optical and Infrared Properties of the Atmosphere, in: *Handbook of Geophysics and the Space Environment*, chap. 18, NTIS, 1985.
- 5 Hale, G. M. and Querry, M. R.: Optical Constants of Water in the 200-nm to 200-microm Wavelength Region., *Applied optics*, 12, 555–563, doi:10.1364/AO.12.000555, 1973.
- Jones, M. R., Leong, K. H., Brewster, M. Q., and Curry, B. P.: Inversion of light-scattering measurements for particle size and optical constants: experimental study, *Applied optics*, 33, 4035–4041, doi:10.1364/AO.33.004035, 1994.
- Jones, S. H., King, M. D., and Ward, A. D.: Determining the unique refractive index properties of solid polystyrene aerosol using broadband Mie scattering from optically trapped beads, *Physical chemistry chemical physics : PCCP*, 15, 20 735–41, doi:10.1039/c3cp53498g, 2013.
- 10 Koehler, K. A., Kreidenweis, S. M., DeMott, P. J., Prenni, A. J., Carrico, C. M., Ervens, B., and Feingold, G.: Water activity and activation diameters from hygroscopicity data - Part II: Application to organic species, *Atmospheric Chemistry and Physics Discussions*, 5, 10 881–10 924, doi:10.5194/acpd-5-10881-2005, 2006.
- Li, J. and Mao, J. T.: Properties of Atmospheric Aerosols Inverted from Optical Remote-Sensing, *Atmospheric Environment Part a-General Topics*, 24, 2517–2522, 1990.
- 15 Lienert, B. R., Porter, J. N., and Sharma, S. K.: Aerosol size distribution from genetic inversion of polar nephelometer data, *Journal of Atmospheric and Oceanic Technology*, 20, 1403–1410, doi:10.1175/1520-0426(2003)020<1403:ASDFGI>2.0.CO;2, 2003.
- Ma, X., Lu, J. Q., Brock, R. S., Jacobs, K. M., Yang, P., and Hu, X.-H.: Determination of complex refractive index of polystyrene microspheres from 370 to 1610 nm., *Physics in Medicine and Biology*, 48, 4165–4172, doi:10.1088/0031-9155/48/24/013, 2003.
- 20 McNaughton, C. S., Clarke, A. D., Howell, S. G., Pinkerton, M., Anderson, B., Thornhill, L., Hudgins, C., Winstead, E., Dibb, J. E., Scheuer, E., and Maring, H.: Results from the DC-8 Inlet Characterization Experiment (DICE): Airborne Versus Surface Sampling of Mineral Dust and Sea Salt Aerosols, *Aerosol Science and Technology*, 41, 136–159, doi:10.1080/02786820601118406, 2007.
- Mishchenko, M. I., Travis, L. D., and Lacis, A. A.: *Scattering, absorption, and emission of light by small particles*, Cambridge university press, 2002.
- 25 Muñoz, O., Moreno, F., Guirado, D., Ramos, J. L., Volten, H., and Hovenier, J. W.: The IAA cosmic dust laboratory: Experimental scattering matrices of clay particles, *Icarus*, 211, 894–900, doi:10.1016/j.icarus.2010.10.027, 2011.
- Nessler, R., Weingartner, E., and Baltensperger, U.: Adaptation of dry nephelometer measurements to ambient conditions at the Jungfraujoch, *Environmental Science and Technology*, 39, 2219–2228, doi:10.1021/es035450g, 2005.
- Orozco, D., Beyersdorf, A. J., Ziemba, L. D., Berkoff, T., Zhang, Q., Delgado, R., Hennigan, C. J., Thornhill, K., Young, D. E., Parworth, C., Kim, H., and Hoff, R. M.: Hygroscopicity Measurements of Aerosol Particles in the San Joaquin Valley, CA, Baltimore, MD, and Golden, CO, *Journal of Geophysical Research: Atmospheres*, 121, 7344–7359, doi:10.1002/2015JD023971, 2016.
- 30 Petters, M. D. and Kreidenweis, S. M.: A single parameter representation of hygroscopic growth and cloud condensation nucleus activity, *Atmospheric Chemistry and Physics*, 7, 1961–1971, doi:DOI:10.5194/acp-7-1961-2007, 2007.
- Pinnick, R. G., Pendleton, J. D., and Videen, G.: Responseor estimating the refractive inde characteristics of the particle measuring systems active scattering aerosol spectrometer probes, *Aerosol Science and Technology*, 33, 334–352, doi:DOI 10.1080/02786820050121530, 2000.
- Redemann, J., Turco, R. P., Liou, K. N., Russell, P. B., Bergstrom, R. W., Schmid, B., Livingston, J. M., Hobbs, P. V., Hartley, W. S., Ismail, S., Ferrare, R. A., and Browell, E. V.: Retrieving the vertical structure of the effective aerosol complex index of refraction from a

- combination of aerosol in situ and remote sensing measurements during TARFOX, *Journal of Geophysical Research: Atmospheres*, 105, 9949–9970, doi:10.1029/1999JD901044, 2000.
- Schuster, G. L., Lin, B., and Dubovik, O.: Remote sensing of aerosol water uptake, *Geophysical Research Letters*, 36, 1–5, doi:10.1029/2008GL036576, 2009.
- 5 SEAC4RS: Studies of Emissions and Atmospheric Composition, Clouds and Climate Coupling by Regional Surveys Data Archive, doi:10.5067/Aircraft/SEAC4RS/Aerosol-TraceGas-Cloud, 2015.
- Shingler, T., Crosbie, E., Ortega, A., Shiraiwa, M., Zuend, A., Beyersdorf, A., Ziemba, L., Anderson, B., Thornhill, L., Perring, A. E., et al.: Airborne characterization of subsaturated aerosol hygroscopicity and dry refractive index from the surface to 6.5 km during the SEAC4RS campaign, *Journal of Geophysical Research: Atmospheres*, 121, 4188–4210, 2016.
- 10 Sultanova, N. G., Nikolov, I. D., and Ivanov, C. D.: Measuring the refractometric characteristics of optical plastics, *Optical and Quantum Electronics*, 35, 21–34, doi:10.1023/A:1021811200953, 2003.
- Svenningsson, B., Rissler, J., Swietlicki, E., Mircea, M., Bilde, M., Facchini, M. C., Decesari, S., Fuzzi, S., Zhou, J., Mønster, J., and Rosenørn, T.: Hygroscopic growth and critical supersaturations for mixed aerosol particles of inorganic and organic compounds of atmospheric relevance, *Atmospheric Chemistry and Physics*, 6, 1937–1952, doi:10.5194/acp-6-1937-2006, 2006.
- 15 Sviridenkov, M. a., Vlasenko, S. S., and Nebosko, E. Y.: Retrieval of the aerosol optical and microphysical parameters from the data of measurements by means of Aurora 4000 nephelometer, in: *Proc. of SPIE, 20th International Symposium on Atmospheric and Ocean Optics: Atmospheric Physics*, edited by Romanovskii, O. A., vol. 9292, pp. 92 922U–1–92 922U–6, doi:10.1117/12.2076156, 2014.
- Tanaka, M., Takamura, T., and Nakajima, T.: Refractive index and size distribution of aerosols as estimated from light scattering measurements, *Journal of Applied Meteorology*, 22, 1253–1261, 1983.
- 20 Tang, I.: Chemical and size effects of hygroscopic aerosols on light scattering coefficients, *Journal of Geophysical Research*, 101, 19 245–19 250, 1996.
- Toon, O. B. and Pollack, J. B.: The Optical Constants of several Atmospheric Aerosol Species: Ammonium Sulfate, Aluminium Oxide, and Sodium Chloride, *Journal of Geophysical Research*, 81, 5733–5748, 1976.
- Toon, O. B., Maring, H., Dibb, J., Ferrare, R., Jacob, D. J., Jensen, E. J., Luo, Z. J., Mace, G. G., Pan, L. L., Pfister, L., Rosenlof, K. H., 25 Redemann, J., Reid, J. S., Singh, H. B., Robert Yokelson, Minnis, P., Chen, G., Jucks, K. W., and Pszenny, A.: Planning, implementation and scientific goals of the Studies of Emissions and Atmospheric Composition, Clouds and Climate Coupling by Regional Surveys (SEAC4RS) field mission, *Journal of Geophysical Research: Atmospheres*, 121, 4967–5009, doi:10.1002/2015JD024297, 2016.
- Volten, H., Munoz, O., Rol, E., Haan, J., W. V., and Hovenier, J.: Scattering matrices of mineral aerosol particles at 441.6 nm and 632.8 nm, *Journal of Geophysical Research*, 106, 17,375–17,401, 2001.
- 30 Westphal, D. L. and Toon, O. B.: Simulations of microphysical, radiative, and dynamical processes in a continental-scale forest fire smoke plume, *Journal of Geophysical Research*, 96, 22 379–22 400, doi:DOI 10.1029/91jd01956, 1991.
- Xu, F., Dubovik, O., Zhai, P.-W., Diner, D. J., Kalashnikova, O. V., Seidel, F. C., Litvinov, P., Bovchaliuk, A., Garay, M. J., van Harten, G., and Davis, A. B.: Joint retrieval of aerosol and water-leaving radiance from multispectral, multiangular and polarimetric measurements over ocean, *Atmospheric Measurement Techniques*, 9, 2877–2907, doi:10.5194/amt-9-2877-2016, 2016.
- 35 Yamasoe, M. a., Kaufman, Y. J., Dubovik, O., Remer, L. a., Holben, B. N., and Artaxo, P.: Retrieval of the real part of the refractive index of smoke particles from Sun/sky measurements during SCAR-B, *Journal of Geophysical Research*, 103, 31 893–31 902, doi:10.1029/98JD01211, 1998.
- Young, A. T.: Revised depolarization corrections for atmospheric extinction, *Applied optics*, 19, 3427–3428, 1980.

Zhao, F.: Determination of the complex index of refraction and size distribution of aerosols from polar nephelometer measurements, *Applied optics*, 38, 2331–2336, 1999.

**Table 1.** Predicted and retrieved real refractive indices, median radii in volume and spherical fractions for the three artificially generated aerosols. Also shown are the deliquescence relative humidities (DRH),  $\kappa$  values, and dry real refractive indices taken from the literature. All refractive indices are at 532nm.

| Compound                            | DRH(%) | Measured RH(%) | $\kappa$  | $r_{50}^{GRASP}$ (nm) | <i>Sphere</i> (%) | $n_{dry}$ | $n_{wet}^{GRASP}$ | $n_{wet}^{\kappa\text{Köhler}}$ |
|-------------------------------------|--------|----------------|-----------|-----------------------|-------------------|-----------|-------------------|---------------------------------|
| <i>NaCl</i>                         | 80     | $83.7 \pm 2$   | 0.91-1.33 | 144                   | 100               | 1.544     | 1.395             | 1.353-1.372                     |
| $(NH_4)_2SO_4$                      | 75     | $82.6 \pm 2$   | 0.33-0.72 | 120                   | 100               | 1.530     | 1.383             | 1.370-1.414                     |
| <i>NH<sub>4</sub>NO<sub>3</sub></i> | 62     | $83.5 \pm 2$   | 0.58-0.75 | 129                   | 54                | 1.554     | 1.392             | 1.371-1.393                     |

**Table 2.** Truncation corrected total scattering ( $\beta_{sca}$ ) from the integrating nephelometer as well as PI-Neph/GRASP retrieved real refractive index, sphere fraction and SSA for the three highlighted case studies. Additionally, the SSA derived from PSAP and integrating nephelometer measurements is shown for comparison. All spectrally dependent parameters are listed at 532nm.

| Aerosol Case | Date                 | Time(UTC)   | $\beta_{sca}$        | $m_{GRASP}$ | <i>Sphere</i> <sub>GRASP</sub> | <i>SSA</i> <sub>GRASP</sub> | <i>SSA</i> <sub>PSAP</sub> |
|--------------|----------------------|-------------|----------------------|-------------|--------------------------------|-----------------------------|----------------------------|
| BB Plume #1  | Aug 19 <sup>th</sup> | 19:06-19:13 | $489\text{Mm}^{-1}$  | 1.594       | 64.5%                          | 0.976                       | 0.964                      |
| BB Plume #2  | Aug 27 <sup>th</sup> | 21:42-21:48 | $95.9\text{Mm}^{-1}$ | 1.565       | 91.0%                          | 0.962                       | 0.959                      |
| Forested BL  | Aug 30 <sup>th</sup> | 20:55-21:12 | $41.9\text{Mm}^{-1}$ | 1.566       | 53.9%                          | 0.908                       | 0.930                      |

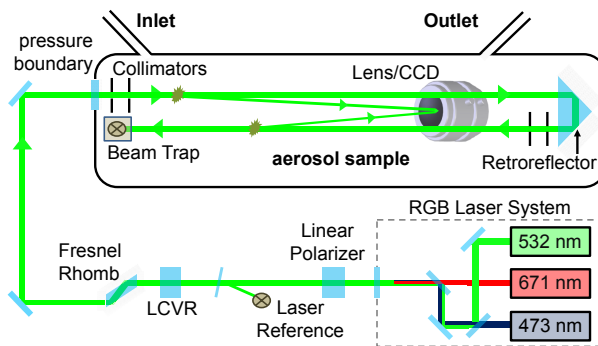


**Figure 1.** The PI-Neph instrument concept. Figure adapted from Dolgos and Martins (2014).

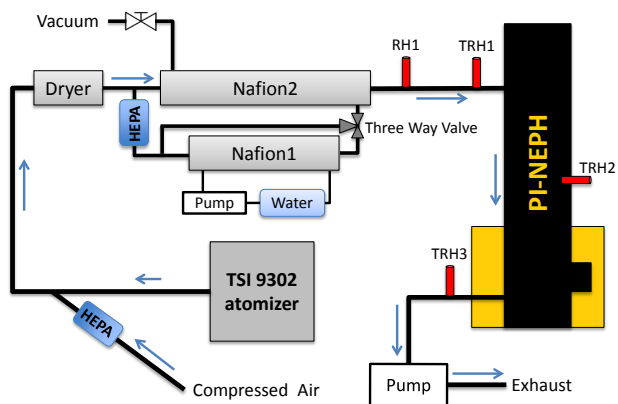


**Figure 2.** Laboratory aerosol generation instrumental setup used to suspend salts and PSL spheres.

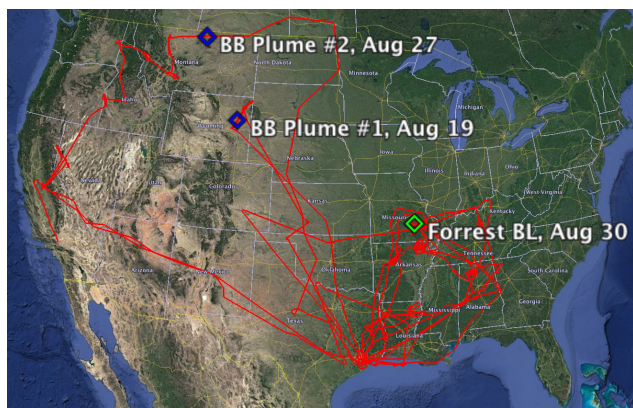


**Figure 3.** Flight paths of the ten SEAC<sup>4</sup>RS flights from which data is used in this paper. Additionally, three specific case studies are called out with diamonds. The case studies include two biomass burning dominated aerosols (blue) as well as measurements made in the boundary layer of a forested region in south east Missouri (green).

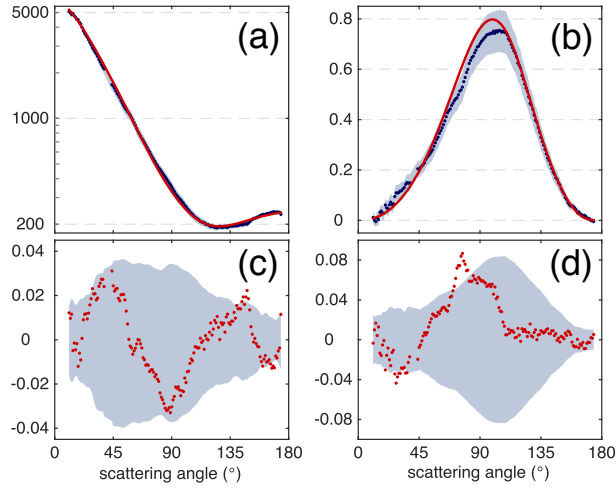


**Figure 4.** PI-Neph measurements at 532nm (points) with  $2\sigma$  instrumental error (gray fill) and the GRASP retrieval best fit (solid line) for ammonium sulfate measurements made in the laboratory. Panel (a) shows absolute  $F_{11}$  ( $Mm^{-1}/sr$ ) data plotted on a log scale, while panel (b) shows  $-F_{12}/F_{11}$  data on a linear scale. Panel (c) shows the  $F_{11}$  differences according to the log transformation described in equation 1, while the conventional residuals in  $-F_{12}/F_{11}$ , as given by equation 2, are plotted in (d).

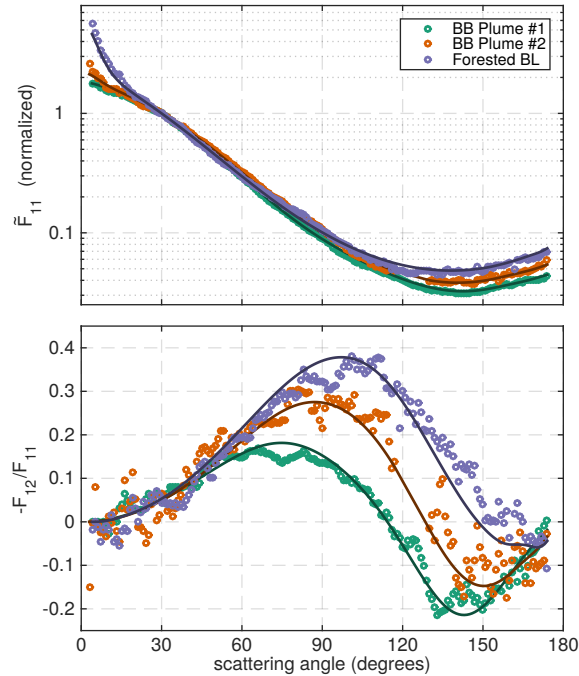


**Figure 5.** Normalized scattering matrix elements (circles) measured by the PI-Neph at 532nm and the corresponding GRASP fits (solid lines) for the three highlighted SEAC<sup>4</sup>RS aerosol samples.

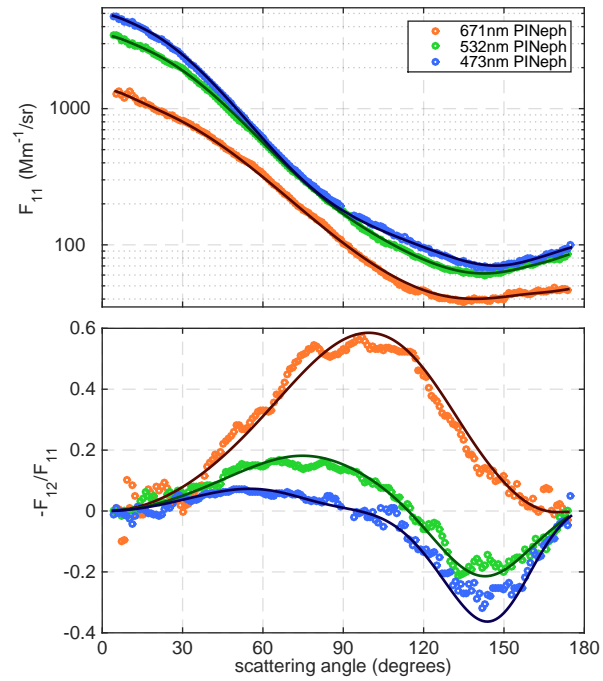


**Figure 6.** Scattering matrix elements at 473nm (blue), 532nm (green) and 671nm (red) measured in BB plume #1 on August 19<sup>th</sup> along with the corresponding GRASP fits (solid lines).

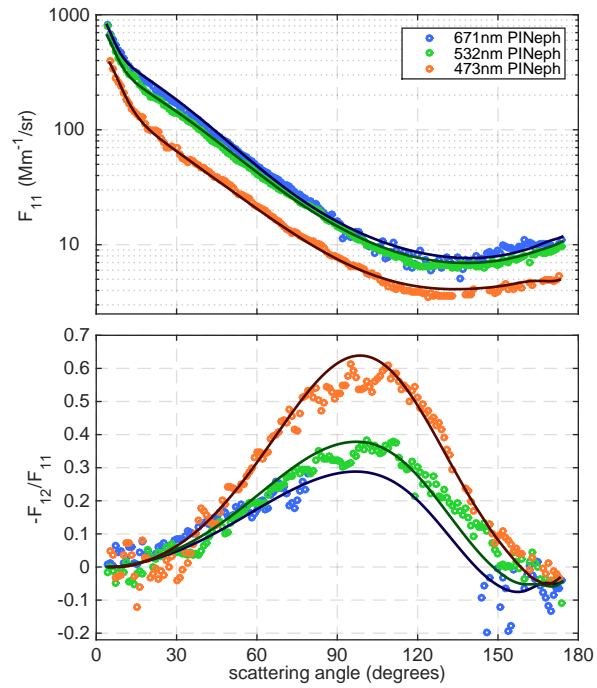


**Figure 7.** Scattering matrix elements at 473nm (blue), 532nm (green) and 671nm (red) measured over a forested region of southeast Missouri along with the corresponding GRASP fits (solid lines).

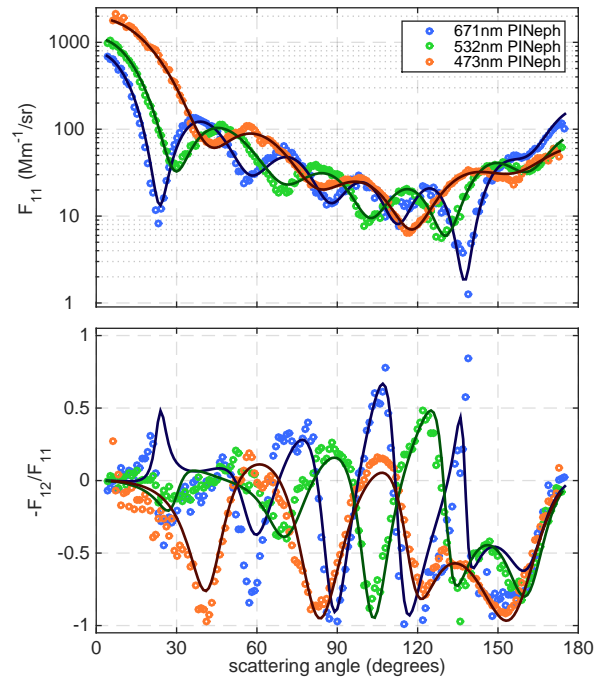


**Figure 8.** Scattering matrix elements at 473nm (blue), 532nm (green) and 671nm (red) for 903nm diameter PSL sample along with the corresponding GRASP fits (solid lines).

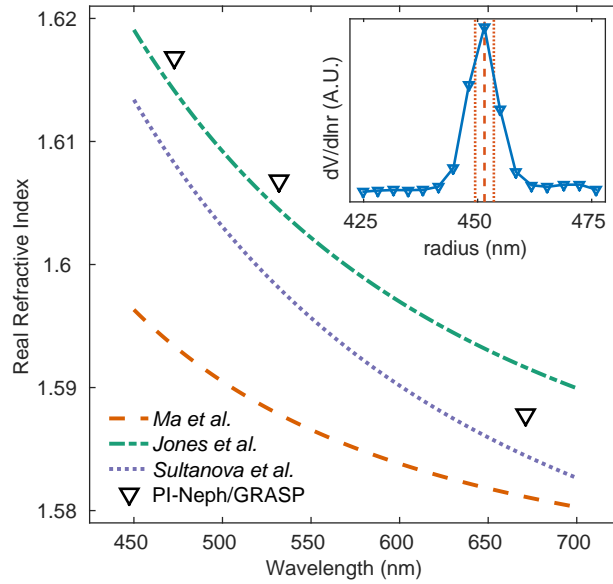


**Figure 9.** Retrieved real part of the refractive index for PSL spheres, alongside three previous, modern measurements of polystyrene refractive indices (Ma et al., 2003; Jones et al., 2013; Sultanova et al., 2003). The subplot shows the retrieved size distribution (blue) along side the manufacturer’s specified central radius (red dashes) and FW67 (red dots).

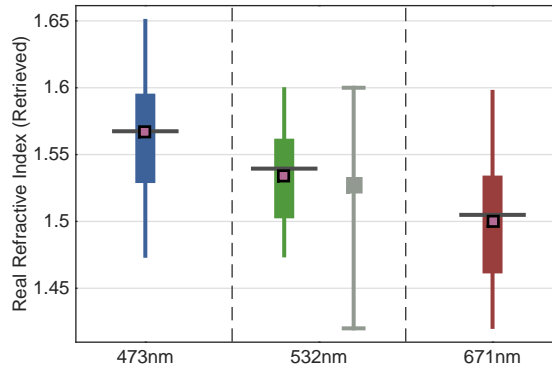


**Figure 10.** Retrieved refractive index at all three PI-Neph wavelengths for the 50 selected SEAC<sup>4</sup>RS samples. Box and whiskers plots show the data distribution by quartile while the connected black squares show the spectral dependence of the mean. The gray bounds at 532nm denote the minimum and maximum values measured by Shingler et al. (2016) in SEAC<sup>4</sup>RS while the grey square denotes the corresponding mean.

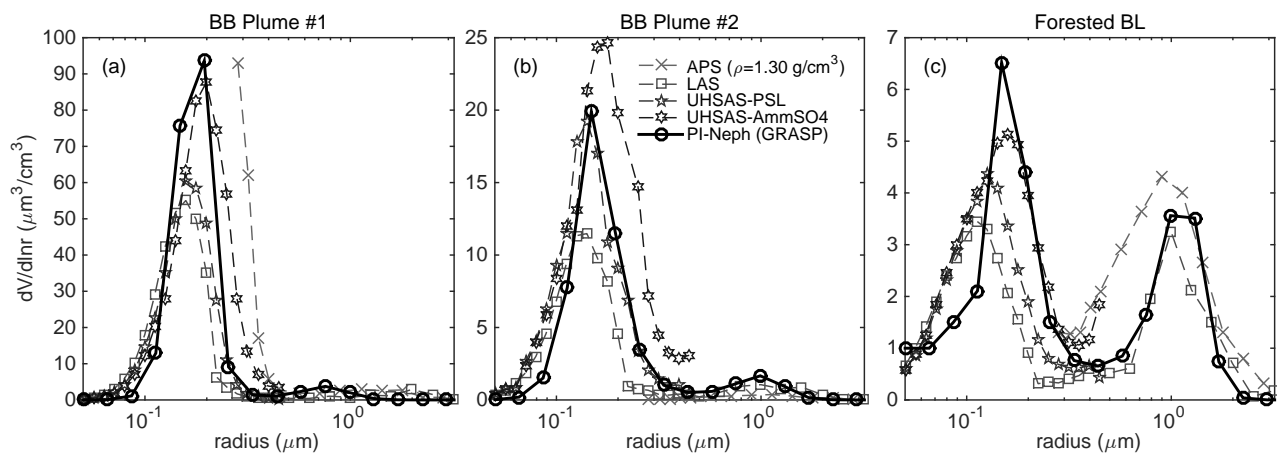


**Figure 11.** Direct comparisons of PI-Neph/GRASP retrieved size distributions with dedicated particle sizers that sampled in parallel to the PI-Neph. The three cases selected show measurements from the (a) August 19<sup>th</sup> and (b) August 27<sup>th</sup> biomass burning cases, as well as (c) boundary layer measurements made above a forested region of southeast Missouri on August 30<sup>th</sup>.

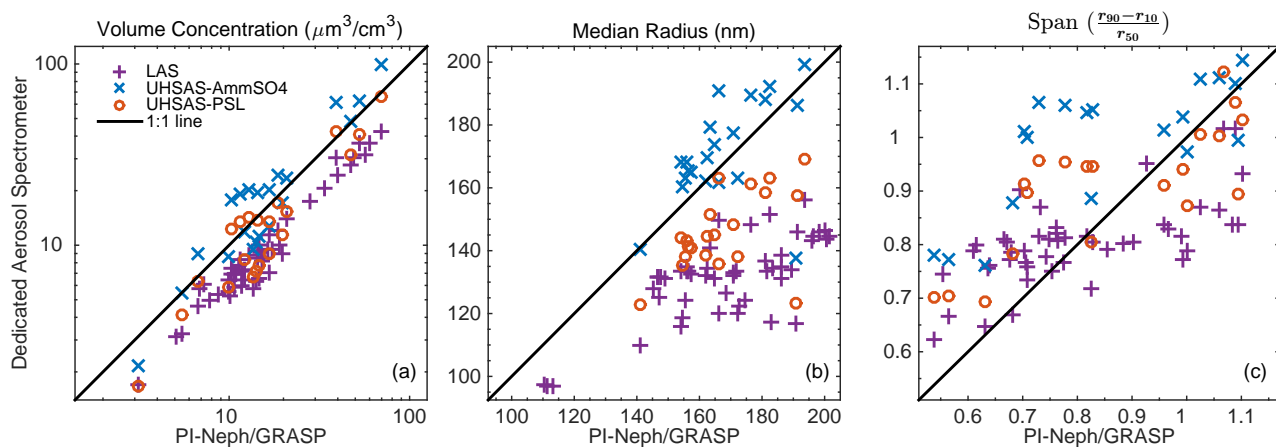


**Figure 12.** Scatter plot comparisons of retrieved size distributions with particle sizers sampling in parallel to the PI-Neph. In order from left to right the panels show total fine mode (a) volume concentration, (b) volume median radius and (c)  $span = \frac{r_{90} - r_{10}}{r_{50}}$ . The value retrieved from PI-Neph measurements is plotted on the horizontal axis while the value measured by the corresponding dedicated aerosol spectrometer is plotted along the vertical axis. The comparisons are made against LAS measurements (purple pluses), UHSAS ammonium-sulfate equivalent optical diameters (blue crosses) and UHSAS PSL equivalent optical diameters (red circles).